

Low-temperature thermal conductivity of the substrate material YAlO_3 and its unconventional sister compound YbAlO_3

Parisa Mokhtari*

*Department of Physics, Technical University of Munich, 85748 Garching, Germany
Max Planck Institute for Chemical Physics of Solids, 01187 Dresden, Germany and
Faculty of Physics, Technische Universität Dresden, 01062 Dresden, Germany*

Ulrike Stockert[†]

Faculty of Physics, Technische Universität Dresden, 01062 Dresden, Germany

Stanislav E. Nikitin

PSI Center for Neutron and Muon Sciences, 5232 Villigen PSI, Switzerland

Leonid Vasylechko

Lviv Polytechnic National University, Lviv 79013, Ukraine

Manuel Brando

Max Planck Institute for Chemical Physics of Solids, 01187 Dresden, Germany

Elena Hassinger

*Faculty of Physics, Technische Universität Dresden, 01062 Dresden, Germany and
Max Planck Institute for Chemical Physics of Solids, 01187 Dresden, Germany*

(Dated: December 3, 2025)

Abstract

We present thermal conductivity data on single crystals of YAlO_3 and YbAlO_3 for temperatures between 2 K and 300 K and the heat current along b and c . Both materials are very good thermal conductors in the investigated temperature range. The thermal conductivity in these electrical insulators is due to phonons. The effect of Y-Yb exchange is found to be rather small despite the considerable difference in density and average atomic mass. For YAlO_3 we find a moderate thermal conductivity anisotropy with weak temperature dependence and a ratio of c to b direction between at most 1 and 2.2. It is discussed with regard to the velocities of sound and relevant scattering processes. For YbAlO_3 the small crystal size limits the precision of absolute thermal conductivity values and does not allow drawing conclusions on the anisotropy. Our results on YAlO_3 confirm that the material is suitable for applications requiring a good thermal conductivity at temperatures down to liquid helium, such as lasers, substrates, and detectors.

I. INTRODUCTION

YAlO_3 is widely used in applications, both as a pure compound and when doped with different elements [1]. Single crystalline YAlO_3 , in literature also referred to as YAP (yttrium aluminum perovskite) is a popular substrate material for growing thin films, for example of high-temperature superconductors [2], heavy-fermion materials [3], and doped perovskites [4]. It has been also suggested as a window material in photodetectors [5]. Cr-doped YAlO_3 , where Cr replaces part of the Al, has been proposed as a temperature sensor material [6], while Mn:YAP is discussed as a candidate for data storage and holographic recording [7, 8]. The largest potential for applications is accomplished by incorporation of rare-earth (RE) ions. RE: YAlO_3 , where part of the yttrium is replaced by elements such as Pr, Nd, Gd, and Yb, are important laser and scintillator materials with possible use in medicine [9, 10], astrophysics [11, 12], and synchrotron technology [13]. A good thermal conductivity is either mandatory or at least advantageous for most of these applications for instance to facilitate energy release in laser materials or thermal coupling of thin films via substrates to the bath. In fact, a good thermal conductivity is expected for high-quality single crystals of YAlO_3 . Experimentally, the thermal conductivity of YAlO_3 has been measured in the temperature range between 80 K and 300 K [14] and between 300 K and 870 K [15]. However,

* Now at Department of Applied Physics and Quantum-Phase Electronics Center, The University of Tokyo, Bunkyo-ku, Tokyo 113-8656, Japan.

† ulrike.stockert@tu-dresden.de

low- T data are missing so far and cannot be extrapolated or estimated from the high-temperature values: The thermal conductivity of insulating single crystals does not change monotonously with temperature but goes through a maximum typically around 10-30 K before approaching zero in the zero-temperature limit. This characteristic T -dependence arises from cumulative phonon excitations upon heating and diverse scattering processes dominating in different T ranges. It depends on sample size and quality [16].

The above-mentioned chemical substitution also has strong influence on the thermal conductivity. Partial substitution of one element by another usually lowers the thermal conductivity via the introduced disorder. Indeed, for Yb:YAlO₃ a significant lowering of the thermal conductivity has been confirmed experimentally [14, 17, 18]. Besides disorder, substitution has also another effect: The difference in atomic mass between the two involved elements changes the density and the phonon spectrum of the material. This effect may be quite large, e.g., exchanging Y with an atomic mass $m_a = 88.9$ u by Yb with $m_a = 173.0$ u increases the density from YAlO₃ to YbAlO₃ by a factor of 1.5. The Debye temperature Θ_D , which is related to the phonon spectrum, is also expected to change, however, literature values are not consistent [14, 19, 20]. Large atomic masses and low Θ_D facilitate low κ values at high T (strictly at $T > \Theta_D$) [21]. In order to disentangle the effects of disorder, effective mass, and Θ_D , thermal conductivity data for YbAlO₃ are needed. At very high $T \gg \Theta_D$ theoretical calculations of the structural and elastic properties predict that the minimum thermal conductivity of YbAlO₃, $\kappa_{\min} = 1.15$ W/Km [22], is significantly lower than the one for YAlO₃ of $\kappa_{\min} = 1.61$ W/Km [23]. The only available experimental κ values for YbAlO₃ are in the milli-Kelvin range in a regime with highly unconventional magnetic phases [24].

In fact, the low- T phase diagram of YbAlO₃ has been studied intensively over the past few years, leading to the discovery of a Luttinger-liquid regime [25], multiple antiferromagnetic phases [26] and several plateau states upon applying magnetic fields [24]. This complex low- T behavior is also reflected in the thermal conductivity. A thorough understanding of κ requires an evaluation of the contribution from phonons, either from an extrapolation from high T data above the exotic region or from a suitable reference compound. These considerations stimulated our interest in the thermal conductivity of YAlO₃ and YbAlO₃ also from a fundamental point of view and beyond its relevance for applications.

In this manuscript we present the thermal conductivity of YAlO₃ between 2 K and 300 K thereby extending the available data range down to liquid He temperatures. We fit the data to the Callaway model and discuss the relevant scattering processes. In addition we show thermal

conductivity data in the temperature window from 50 K to 300 K on YbAlO_3 for which the change in average atomic mass and also density compared to YAlO_3 is very large and only exceeded marginally by the one of LuAlO_3 . Finally, we discuss the differences between the Y and Yb compounds as well as implications for applications. We also comment on the relevance of our results for understanding the low- T thermal conductivity of YbAlO_3 .

II. EXPERIMENTAL TECHNIQUES

Oriented single crystals of YAlO_3 grown by the Czochralski technique were bought from CRYSTAL GmbH, Berlin (lattice constants: $a = 5.18027 \text{ \AA}$, $b = 5.32951 \text{ \AA}$, and $c = 7.37059 \text{ \AA}$). A single crystal of YbAlO_3 (lattice constants: $a = 5.126 \text{ \AA}$, $b = 5.331 \text{ \AA}$, and $c = 7.313 \text{ \AA}$) was grown by a Czochralski technique as described elsewhere [27]. The orientation of the YbAlO_3 crystal was initially determined by Laue diffraction and subsequently confirmed by magnetization measurements at low T making use of the large angular dependence of the magnetic properties of the material [25]. The oriented crystals were cut into cuboid bars, with dimensions given in Table I.

It needs to be noted that the orientation convention for YAlO_3 and related materials is not uniform in literature [28], which becomes important when comparing results for different crystallographic directions. Throughout this manuscript we use the Pbnm setting of space group N 62, where $c > b \geq a$.

The thermal conductivity κ was measured using a standard steady-state method with a two-thermometer-one-heater configuration in the T range of 2 K - 300 K in a commercially available Quantum Design (QD) Physical Property Measurement System (PPMS). Two calibrated Cernox chip resistors sitting on gold-plated copper shoes were used as thermometers to determine the average sample temperature and the temperature difference along the sample. The heat current j_Q was applied $\parallel b$ (κ_b) and $\parallel c$ (κ_c). To ensure thermal coupling of the contacts to the electrically insulating samples, four micro-contacts consisting of a 10 nm titanium layer covered by a 150 nm gold layer were sputtered onto each sample. One end of the samples was clamped at the cold bath. The contacts to the thermometers and the heater were accomplished via gold-plated copper bars glued to the sample contact pads with silver paint and clamped to the thermometer shoes by screws. The values for the mean distance $l_{\Delta T}$ between the cold and hot probes are given in Table I. The finite contact widths $\delta l_{\Delta T}$ of about 0.2 mm and the measurement accuracy of the sample

Table I. Dimensions and contact geometries of the measured samples. l_a , l_b , and l_c are the sample lengths along the a -, b -, and c -axis, respectively. $l_{\Delta T}$ is the mean distance between the cold and hot probes.

Sample	$(l_a \times l_b \times l_c)$ (mm ³)	\vec{j}_Q	$l_{\Delta T}$ (mm)
YAlO ₃ #b	$0.5 \times 5 \times 0.5$	$\parallel b$	2.7
YAlO ₃ #c	$0.5 \times 0.5 \times 5$	$\parallel c$	2.7
YbAlO ₃ #b	$0.45 \times 2 \times 0.45$	$\parallel b$	1.2
YbAlO ₃ #c	$0.5 \times 0.5 \times 1.95$	$\parallel c$	1.15

dimensions of about ± 0.01 mm sum up to a considerable uncertainty of the geometry factor and in consequence of the absolute values of κ , upper limits being about 11 % for YAlO₃ and 21 % for YbAlO₃. This systematic error does not affect the shape of $\kappa(T)$, but enters only as a prefactor changing the absolute κ values. However, a discussion of differences or the anisotropy of κ is not reasonable below these thresholds.

In order to avoid excessive heat loss from thermal radiation during measurements, the rise of the average sample temperature T_{av} was limited to about 3 % compared to the bath temperature. Depending on the thermal coupling between sample and bath and the sample geometry, the resultant temperature difference between warm and cold probe for YAlO₃ was typically within 1 % and 3 % of T_{av} .

The radiation loss was estimated from the sample temperatures at the hot and cold contacts, the bath temperature, the sample surface area, and a rough value for the emissivity of the materials of 0.5. Around 250 K the calculated radiation loss exceeds 1 % of the heater power and reaches at most 2.5 % close to room temperature. However, we know from experiments, where we compared thermal conductivity data obtained with different methods, that radiation losses are underestimated by our correction procedure and may get important already above about 200 K [29]. Therefore, we included a term accounting for radiation losses in our model.

For YbAlO₃ the very high thermal conductivity in combination with the small sample size led to extremely small or even unresolvable temperature gradients below about 50 K. Despite our efforts to improve the thermal coupling by using gold-plated contacts, we were not able to obtain reproducible data for this material at lower T . Therefore, we restrict our presentation and discussion in this case to temperatures above 50 K, i.e. covering the regime of liquid nitrogen, which is still an important temperature range for applications.

III. RESULTS AND DISCUSSION

A. Heat transport in YAlO_3

Fig. 1 shows the thermal conductivity of YAlO_3 measured for the heat current j_Q along b (κ_b) and along c (κ_c). The inset depicts the same data in a double logarithmic presentation in comparison to results from literature explained in detail below. The results for YAlO_3 can be directly compared to the equivalent data of YbAlO_3 shown in Fig. 2, that will be presented in the next section.

The thermal conductivities κ_b and κ_c of YAlO_3 have very similar temperature dependencies, although with slightly different absolute values. They strongly increase with increasing temperature, go through huge maxima at about 25 K and decrease rapidly towards higher T . The values at the maximum are about 20 times larger than those in SrTiO_3 , another popular substrate material with perovskite structure [30]. They also exceed those measured on isostructural NdGaO_3 , and the related NdAlO_3 and LaAlO_3 by a factor of about 5 [31, 32]. However, they are still well below those reached by other common substrate materials with different structure as silicon and sapphire, reaching 4 000 W/Km and more than 10 000 W/Km, respectively [33, 34].

The observed type of T dependence is typical for clean, nonmetallic, and nonmagnetic single crystals: Thermal transport is purely phononic and limited by boundaries and defects at lowest T . At low T κ increases due to cumulative excitation of phonons. The maximum at mid T arises due to the onset of umklapp (U) scattering of phonons with large momentum leading to a decreasing mean free path up to room temperature.

The thermal conductivity is smaller for $j_Q \parallel b$. It can be roughly scaled to the one for $j_Q \parallel c$ by a factor of 1.35. The ratio κ_c/κ_b is plotted in Fig. 3 and discussed in more detail below. Our observation of an only moderate anisotropy is in accordance with literature results [14, 15]. However, the relative size differs: While $\kappa_c > \kappa_b$ in our study in line with Ref. 15, an opposite anisotropy with $\kappa_b > \kappa_c$ has been claimed in Ref. 14. This latter proportion has been challenged by A. Hofmeister [35]: Based on thermal diffusivity measurements on YAlO_3 and related compounds the author concluded that the notation of the YAlO_3 crystal axes was permuted in Ref. 14. This suggestion is in fact in perfect agreement with our finding as demonstrated in the inset of Fig. 1. It compares the data from Ref. 14, however, with the orientation labeled according to Ref. 35 to our thermal conductivity. Both data sets have similar values and anisotropy. In addition we plot the

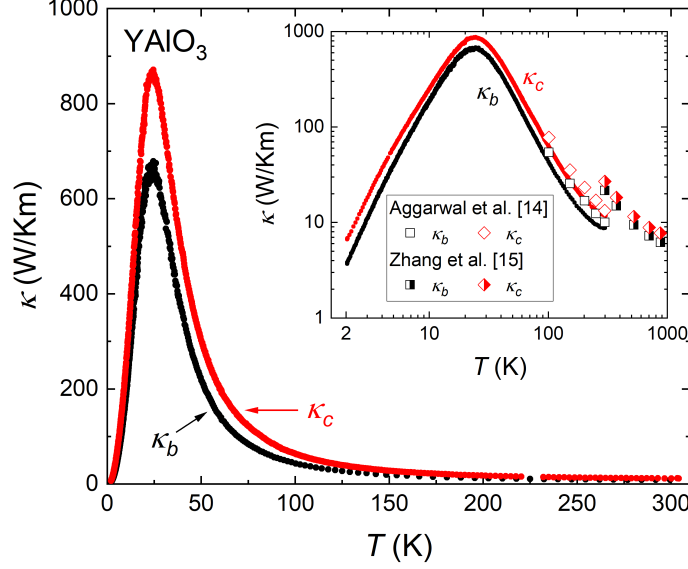


Figure 1. Temperature dependence of the thermal conductivity κ of YAlO_3 along the b -axis (κ_b) and the c -axis (κ_c) plotted in black and red, respectively. The inset presents the same data on a double-logarithmic scale in comparison to literature data from Aggarwal *et al.* [14] and Zhang *et al.* [15].

high-temperature results from Ref. 15, which have somewhat larger absolute values but a similar anisotropy and T dependence.

The remaining differences between results from different groups may be due to measurement uncertainties, especially for sample dimensions. As mentioned in the experimental section, our geometry factor for YAlO_3 and in consequence absolute κ values are only known within $\pm 11\%$. Uncertainties from other sources may be neglected in our case. On the other hand, the thermal conductivity data in Ref. 14 and 15 were obtained from diffusivity and specific heat measurements, the accuracy of which is estimated in Ref. 14 to be 7% for each quantity. The respective data sets can be scaled to ours by a factor of roughly 0.77, which is within the combined uncertainty of absolute values. The deviations of the data in Ref. 15 are much larger, however no details on the measurement accuracy are specified.

In this context one may ask, whether the observed anisotropy $\kappa_c/\kappa_b \approx 1.35$ is an established fact or whether it might be attributed to measurement uncertainties as well. The range of $\pm 11\%$ for our absolute κ values for an individual sample corresponds to an uncertainty of 22% for the ratio between two different measurements. However, this value represents the worst case and is unlikely to be realized. Moreover, it is still too small to fully account for the difference between κ_b and κ_c . This is demonstrated in Fig. 3, which compares the ratio κ_c/κ_b for different data sets

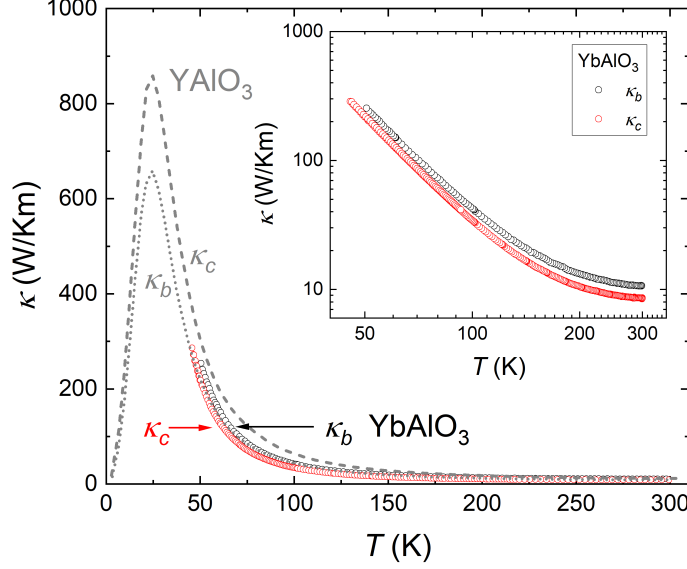


Figure 2. Temperature dependence of the thermal conductivity κ of YbAlO_3 along the b -axis (κ_b) and the c -axis (κ_c) plotted in black and red, respectively. Data for YAlO_3 are shown as dashed lines for comparison. The inset presents the YbAlO_3 data on a double-logarithmic scale.

including estimates of the maximum uncertainty range for selected data points. The isotropic value $\kappa_c/\kappa_b = 1$ is marked by a dashed line and lies below the uncertainty range for YAlO_3 except for a small window around 20 K. Moreover, the anisotropy ratio κ_c/κ_b strongly increases below 10 K to about 1.8 at 2 K. Such a temperature dependence cannot be attributed to measurement uncertainties of the contact geometry. In combination with the very similar anisotropy observed in previous studies, this allows us to conclude that the thermal conductivity of YAlO_3 indeed exhibits a moderate anisotropy κ_c/κ_b with a weak temperature dependence below room temperature.

B. Heat transport in YbAlO_3

The thermal conductivity of YbAlO_3 is shown in Fig. 2. For comparison, the data of YAlO_3 are added as lines. The inset of Fig. 2 plots the same data on a double logarithmic scale. As mentioned in the experimental section, measurements on YbAlO_3 were not successful below about 50 K due to the large thermal conductivity and the small crystal size. The behavior of κ_b and κ_c of YbAlO_3 is very similar to the one of YAlO_3 , both for the T -dependence and the absolute values. The latter observation is somewhat unexpected in view of the considerable difference of the minimum thermal conductivities κ_{\min} predicted from density functional theory (DFT) calculations of elastic

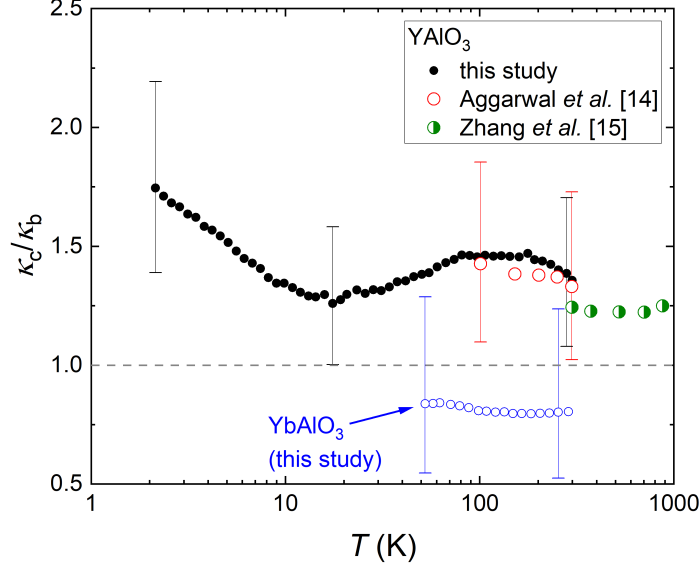


Figure 3. Temperature dependence of the thermal conductivity ratio κ_c/κ_b of YAlO_3 and YbAlO_3 including literature data from Aggarwal *et al.* [14] and Zhang *et al.* [15] on YAlO_3 . The error bars demonstrate maximum uncertainties from the upper and lower bounds for the geometry factors and measurement techniques. No respective estimate is provided by Zhang *et al.*

constants and the model proposed by Clarke, namely 1.61 W/Km for YAlO_3 compared to 1.15 W/Km for YbAlO_3 [22, 23, 36]. However, the regime of κ_{\min} is only reached at temperatures well above the Debye temperature Θ_D , i.e. far above our measurement range.

The very similar magnitude and temperature dependence of κ for YbAlO_3 and YAlO_3 in the T range above 50 K points to a rather uniform behavior also at lower T . Therefore, we suspect, that YbAlO_3 is a very good thermal conductor down to temperatures of liquid He with a maximum in κ around 20-30 K. This assumption is also supported by the fact that we could not recover a sizable thermal gradient at lower T in our setup, meaning that the thermal conductivity stays indeed large down to 2 K. However, absolute values at low T cannot be evaluated from high- T data, because different scattering processes dominate in the respective regimes. This is discussed in more detail below.

Another interesting point is the anisotropy of κ . For YbAlO_3 $\kappa_c < \kappa_b$, which is opposite to the anisotropy for YAlO_3 . The temperature dependent ratio κ_c/κ_b of YbAlO_3 is shown in Fig. 3 including estimates for the maximum uncertainty range of absolute values. From this plot it is clear, that a discussion of the anisotropy of κ of YbAlO_3 is not reasonable based on our data because of the uncertainty of the geometry factors. While YbAlO_3 has most likely a smaller ratio

κ_c/κ_b than YAlO_3 above 50 K with an only weak T dependence, we cannot draw any conclusion about the absolute values, in particular whether κ_c/κ_b is larger or smaller than 1.

C. Discussion

As mentioned above, the temperature dependencies of $\kappa(T)$ for YAlO_3 and YbAlO_3 are typical for electrically insulating single crystals. In the following we discuss the data in more detail focusing on the origin of the anisotropy of κ and its temperature dependence in YAlO_3 .

A simple scenario to explain a thermal transport anisotropy is a direction-dependence of the sound velocity v . Starting with the kinetic relation $\kappa = 1/3 c_V v \lambda = 1/3 c_V v^2 \tau$, with c_V being the specific heat at constant volume, one may assume either an isotropic mean free path λ yielding an anisotropy $\kappa_c/\kappa_b = v_c/v_b$ or an isotropic scattering time τ corresponding to $\kappa_c/\kappa_b = v_c^2/v_b^2$. Since there is no experimental report on the direction-dependent velocities of sound of neither YAlO_3 nor YbAlO_3 , we use two routes for an estimation: (1) from the elastic constants and (2) from phonon dispersion curves. For the first estimation we take the elastic constants calculated by an *ab initio* DFT method by Zhan *et al.* (YAlO_3) [23] and Xiang *et al.* (YbAlO_3) [22] to compute the sound velocities along different principal axes. For each crystallographic direction of ijk (e.g. the i -axis), one may define one longitudinal velocity v_l (v_{ii}) and two transverse velocities of v_{t1} ($v_{i,j}$) and v_{t2} ($v_{i,k}$). For an orthorhombic crystal structure, the relation to the elastic constants reads: [37]

$$\hat{v} = \begin{pmatrix} v_{i,i} & v_{i,j} & v_{i,k} \\ v_{j,i} & v_{j,j} & v_{j,k} \\ v_{k,i} & v_{k,j} & v_{k,k} \end{pmatrix} = \frac{1}{\sqrt{\rho}} \begin{pmatrix} \sqrt{c_{11}} & \sqrt{c_{66}} & \sqrt{c_{55}} \\ \sqrt{c_{66}} & \sqrt{c_{22}} & \sqrt{c_{44}} \\ \sqrt{c_{55}} & \sqrt{c_{44}} & \sqrt{c_{33}} \end{pmatrix} \quad (1)$$

where ρ is the density, c_{11} , c_{22} , and c_{33} represent stiffness against uni-axial strains, and c_{44} , c_{55} , and c_{66} correspond to shear deformations. Once the longitudinal and transverse velocities are known, an estimate for the mean sound velocity for a specific direction can be found via $\bar{v}_i^{-3} = (v_{i,i}^{-3} + v_{i,j}^{-3} + v_{i,k}^{-3})/3$, which is strictly valid only for isotropic materials. The results are given in Table II, together with the overall average sound velocities \bar{v} calculated as the geometric mean of the three directions and the thermal conductivity anisotropies determined as $\kappa_c/\kappa_b = \bar{v}_c^2/\bar{v}_b^2$.

The second method can be applied only for YAlO_3 , since no phonon dispersion curves have been published for the Yb compound. Theoretical phonon dispersion curves for YAlO_3 at room temperature have been obtained from a rigid ion model and Raman results [38] as well as from *ab initio* calculations using the VASP and phonopy codes [39]. The sound velocities calculated

Table II. Mean sound velocities for YAlO_3 and YbAlO_3 along the three crystallographic axes calculated from the elastic tensor ϵ or phonon dispersion curves (PhDis) and resultant overall average sound velocity \bar{v} and thermal conductivity anisotropy $\kappa_c/\kappa_b = \bar{v}_c^2/\bar{v}_b^2$.

Material	source	\bar{v}_a (m/s)	\bar{v}_b (m/s)	\bar{v}_c (m/s)	\bar{v} (m/s)	κ_c/κ_b
YAlO_3	ϵ [23]	6020	5410	5460	5640	1.02
YAlO_3	PhDis [38]	6110	4920	5510	5530	1.25
YAlO_3	PhDis [39]	5120	5220	5750	5370	1.21
YbAlO_3	ϵ [22]	3890	3930	4410	4080	1.26

from the slopes of the acoustic branches and resultant values for \bar{v} and κ_c/κ_b are also presented in Table II.

We start with the results for YAlO_3 : Two findings are interesting with respect to our thermal conductivity measurements. First, the overall average sound velocities \bar{v} are close to each other for all methods of calculation and only slightly larger than the polycrystalline average sound velocity of 5290 m/s calculated by Zhan *et al.* based on the Voigt, Reuss, and Hill approximations [23, 40–42]. Second, the anisotropy of the sound velocities depends on the method of estimation. In particular, the calculation from the elastic constants reveals an almost isotropic behavior along b and c and slightly larger value along the a -axis. This is even more remarkable in view of the considerable anisotropy of the elastic constants, e.g. $c_{cc}/c_{bb} = c_{33}/c_{22} = 0.78$. Apparently, they cancel out when averaging over longitudinal and transverse components. As result, the ratio of the mean sound velocities calculated from the elastic constants cannot explain the observed thermal transport anisotropy of YAlO_3 , neither for an isotropic mean free path ($\bar{v}_c/\bar{v}_b = 1.01$) nor an isotropic scattering time ($\bar{v}_c^2/\bar{v}_b^2 = 1.02$). We attribute this to the approximations used in the model. By contrast the sound velocities obtained from the phonon dispersion curves are in line with a larger thermal conductivity along c than along b , and the anisotropies $\kappa_c/\kappa_b = \bar{v}_c^2/\bar{v}_b^2$ of about 1.2 calculated assuming an isotropic τ are comparable to the experimental one, although the temperature dependence cannot be explained by this simple estimate.

Next we look at YbAlO_3 . All calculated sound velocities are considerably smaller than for YAlO_3 . This is in contradiction to our experimental finding of similar κ values for both compounds given the simple proportionality $\kappa \propto v$ or $\kappa \propto v^2$. Moreover, the anisotropy κ_c/κ_b for

YbAlO₃ predicted by the velocities is opposite to our results. While part of the discrepancies may be caused by the considerable uncertainty of our absolute κ values, the applied simplifications of reducing the full phonon dispersion relation to three sound velocities are probably too coarse and additional parameters, as a temperature and orientation dependence of the mean free path or anharmonic effects need to be taken into consideration. For instance, the above mentioned DFT calculations also predict a significant difference of the Grüneisen parameter between the Y and Yb compound [22, 23]. This parameter is used in describing anharmonic scattering processes and can have a considerable effect on κ [43]. However, the calculated values represent a high- T limit and are thus of limited validity in our investigated T range. Likewise, the elastic constants used in the estimation of the sound velocities are susceptible to the approximations and simplifications immanent to the applied model. Most important, the DFT calculations are performed for $T = 0$ and cannot describe any T -dependence.

In order to understand the temperature dependence of the thermal conductivity anisotropy, different scattering processes and their T dependence have to be taken into account. At very low temperatures, phonons are predominantly scattered by sample or grain boundaries. In first approximation, this regime is characterized by a constant mean free path λ and a cubic T dependence of κ . For YAlO₃ λ can then be determined from the kinetic relation using specific heat data and an average value for the sound velocity of 5500 m/s. Fig. 4 shows the YAlO₃ data again in a double logarithmic presentation together with dotted lines illustrating the respective behavior. The thermal conductivity range, which may be approximated by this simple relation is limited to below at most 4 K. Our estimates for the phonon mean free paths at low T for $j_Q \parallel b$ and c are 17 μm and 29 μm , respectively. These values are about one order of magnitude below the minimum sample dimension indicating that thermal transport at low T is limited by defects and not the sample size. Moreover, the rather poor agreement between a simple cubic behavior and our data demonstrates, that other scattering centers besides boundaries are relevant. Nevertheless, the rather large values for the phonon mean free path at low T confirm the high purity of the investigated single crystals.

At higher temperatures, additional scattering mechanisms become relevant. A phenomenological model frequently used to analyze the relevance of different scattering processes in the thermal conductivity has been proposed by Callaway [44]. This model is based on the relaxation time and Debye approximations. The original version does not take into account dispersion and anisotropies of the sound velocity or phonon spectrum. It has been subsequently expanded to deal with more complex situations, see e.g., Ref. 45–47. In order to limit the number of free parameters, we stick

to the original variant of this model, assuming an isotropic velocity of sound. The total lattice thermal conductivity is determined from a combined relaxation time τ_c defined as $\tau_c^{-1} = \tau_q^{-1} + \tau_N^{-1}$ with τ_q and τ_N as the phonon scattering times via resistive and nonresistive (normal) 3-phonon-processes, respectively. Although nonresistive, normal processes do not limit thermal conduction directly, they are relevant as they affect the phonon distribution function. The temperature and frequency dependence of τ_N is calculated from $\tau_N^{-1}(\omega, T) = NT^\alpha \omega^\beta$ with $\alpha = 2$, $\beta = 3$, and N as a free parameter. τ_q in turn is determined from all individual resistive scattering rates. In our case we consider scattering at the sample boundaries (τ_b), at point defects (τ_{def}), at dislocations (τ_{dis}), and due to phonon-phonon U-scattering processes (τ_U). Thus $\tau_q^{-1} = \tau_b^{-1} + \tau_{\text{def}}^{-1} + \tau_{\text{dis}}^{-1} + \tau_U^{-1}$, which reads in more detail:

$$\tau_q^{-1}(\omega, T) = \frac{\bar{v}}{l} + A\omega^4 + D\omega + BT^\alpha \omega^\beta \exp\left(-\frac{\Theta_D}{bT}\right) \quad (2)$$

with the terms representing the individual scattering times in the respective order. \bar{v} and l are the average velocity of sound and the mean sample cross-section dimension. The exponents α and β are the same as for normal processes. A , D , B , and b are free parameters of the model. In our calculation of κ we also include a contribution with cubic T dependence cT^3 for possible radiation losses at high T .

Some values of equation 2 can be determined prior to modeling. As mean sample cross-section dimension we use $l = \sqrt{4A_s/\pi}$ with the cross-section A_s . For the average sound velocity \bar{v} we take a value of 5500 m/s corresponding to an average from the elastic constants and the phonon dispersion estimates. The situation is more difficult for the Debye temperature Θ_D as literature values vary significantly. The shift of phonon lines in a photoluminescence study yielded $\Theta_D = 465$ K [19]. Fits of the temperature-dependence of the lattice parameters a and c resulted in values of 440 K and 466 K with rather large uncertainties of about ± 90 K, while the respective value for the b lattice parameter of about 900 K is most probably overestimated [20]. The corresponding evolution of the unit-cell volume yielded $\Theta_D = 545$ K. From specific heat measurements a Debye temperature of 760 K was determined [14]. Balancing the large spread of literature values for Θ_D and our aim to reduce the number of parameters in equation 2 we decided to model our thermal conductivities for two fixed values, namely 460 K and 760 K. This procedure also allows some estimation of the stability of the other parameters.

Having reduced the number of free parameters from 9 to 6 we modeled our thermal conductivity data for YAlO_3 by sampling the parameter space incrementally. As criterion for the agreement

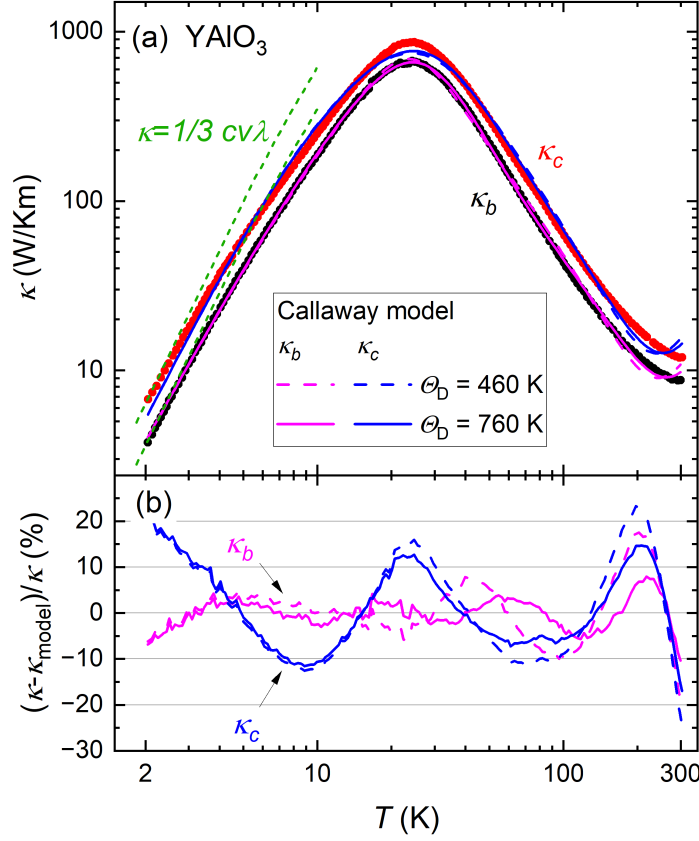


Figure 4. (a) The upper panel shows the results of modeling the thermal conductivities κ_b and κ_c of YAlO_3 by the Callaway model. The calculated curves for κ_b can be barely distinguished from the data and from each other, except for the range $T > 200$ K. For κ_c , systematic deviations between model and data are seen at all T . Details of the calculation procedure are given in the main text. The corresponding parameters are summarized in Table III. The dotted lines at low T demonstrate the behaviors expected from the kinetic relation for constant mean-free paths λ . (b) The lower panel shows the deviations between model and data, emphasizing the much better agreement between for κ_b than for κ_c .

between model and data we used the root mean square deviation RMSD in a double logarithmic presentation. In order to consider the whole measurement range with equal relevance, we averaged our original data set with a step width of 3% in temperature. This procedure yielded the same number of data points for both orientations.

Fig. 4a shows the best descriptions of our data sets for $\Theta_D = 460$ K and $\Theta_D = 760$ K. The corresponding model parameters and RMSD values are summarized in Table III. The uncertainties indicate the width of 2 RMSD determined by separately varying each parameter. I.e., these values

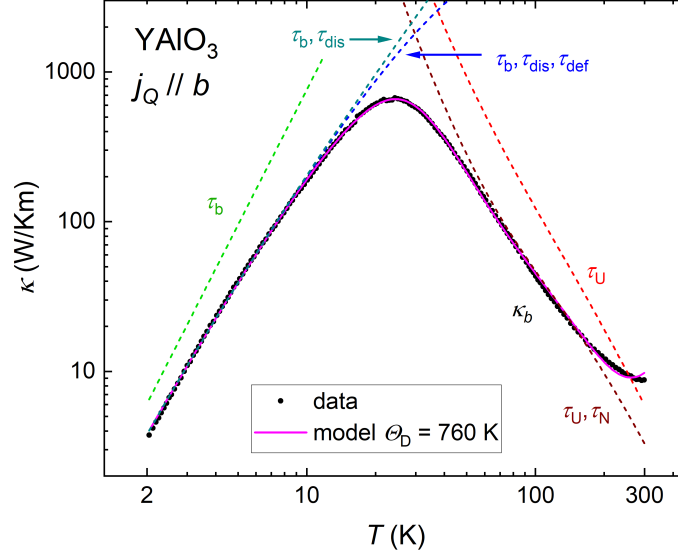


Figure 5. Influence of the different scattering contributions on the thermal conductivity of YAlO_3 for $j_Q \parallel b$ using $\Theta_D = 760$ K. The dashed lines correspond to situations when only the specified relaxation times are taken into account.

Table III. Best parameters found to describe the T dependence of κ for YAlO_3 in a double-logarithmic presentation by the Callaway model. The root mean square deviation RMSD is a measure for the deviation of model and data.

Sample	Θ_D	N	A	D	B	b	c	RMSD
	(K)	(10^{-22} s/K ³)	(10^{-46} s ³)	10^{-6}	(10^{-23} s/K ³)		10^{-7} W/mK ⁴	
		normal	point	dislocations	umklapp	umklapp	radiation	
		processes	defects		scattering	scattering	losses	
YAlO ₃ #b 460	25 (> 3)	0.7 (< 3.7)	5.2 ± 1.3	6.7 ± 1.3	12.3 ± 3.8	3.1	0.026	
YAlO ₃ #b 760	8 (4 – 40)	3.9 ± 1.5	5.1 ± 0.7	8.2 ± 1.0	12.1 ± 1.8	2.4	0.013	
YAlO ₃ #c 460	< 0.4	80 (20 – 180)	1.5 ± 1.4	9.0 ± 3.4	13.5 (7 – 37)	4.5	0.046	
YAlO ₃ #c 760	< 0.4	80 (30 – 160)	1.5 ± 1.2	11.0 ± 3.2	17.6 (12 – 30)	3.7	0.037	

do not take into account mutual dependencies and are merely meant to give an impression of the parameter precision. In some cases, only an upper or lower limit is specified. A missing lower limit for A and N means that the respective scattering process can be ignored without reducing the fit quality significantly. The absence of an upper limit for N implies that even infinitely rapid

normal processes are in line with the data.

For κ_b , the agreement between calculated curves and data is very good given the simplicity of the model. In fact, the model curves can be barely distinguished from the data and from each other on the scale of Fig. 4a, except for the region above about 200 K. This is also seen in Fig. 4b showing the relative difference between data and model. In a large T range it is well below 10 %, exceeding this value only above 150 K. These deviations at high T cannot be explained satisfactorily by radiation losses with cubic temperature dependence, an effect, which was included in our model and is responsible for the upturn in the calculated curves at highest T . Instead, we suspect that the Debye approximation is no longer a good description of the phonon spectrum in this T range, for instance due to an increasing contribution from anharmonic effects or optical modes. The latter is in line with the observation of a low-lying Einstein mode in thermal expansion measurements [20]. The characteristic Einstein temperature was found to be about $230 \text{ K} \pm 130 \text{ K}$, i.e., it might be relevant for the thermal conductivity above 200 K.

In contrast to κ_b , κ_c could not be modeled satisfactorily. The calculated curves show systematic deviations from the data, independent of the choice of Θ_D . This is also visible from the relative deviation between data and model for κ_c in Fig. 4b, which is much larger than for κ_b and oscillates in the whole investigated T range meaning that there is a systematic deviation of the data from the model. Moreover, the parameter set for the best description is almost the same for $\Theta_D = 460 \text{ K}$ and 760 K , cf. Table III. Either additional scattering mechanisms play a role, or the Debye approximation and an isotropic sound velocity are not compatible with the observed anisotropy of the thermal conductivity of YAlO_3 .

The influence of the different scattering contributions on the thermal conductivity of YAlO_3 is demonstrated exemplarily for κ_b and $\Theta_D = 760 \text{ K}$ in Fig. 5. The low- T part of κ is defined by a combination of scattering from sample boundaries and dislocations. At high T the thermal conductivity is predominantly limited by normal and umklapp scattering processes. Point defects are of minor importance in the whole investigated temperature range. In particular, the mean free path at lowest T estimated above to be $\approx 20 \mu\text{m}$ is mostly limited by dislocations. It may be somewhat unexpected that the corresponding fit parameter for defect scattering is anisotropic. However, we may not exclude, that our YAlO_3 crystals stem from different batches with a different impurity concentration. At this point we would also like to recall, that there is a considerable mutual dependence between the fit parameters for scattering processes dominating at low T , namely from boundaries, point defects, and dislocations, and for those relevant at high T , i.e. umklapp and

normal scattering processes.

It is not reasonable to model the thermal conductivity of YbAlO_3 in the same way as for YAlO_3 . Our calculations for YAlO_3 reveal a poor reproducibility of the data by the model above 200 K, most probably due to limitations of the Debye approximation. In combination with the reduced measurement region for YbAlO_3 the T range for modeling is simply too small to get reliable results for this material. This precludes also an extrapolation of our data to very low temperatures to get a good estimate of the phonon contribution to the thermal conductivity in the milli-Kelvin region. A different approach has to be taken in order to disentangle the magnetic and lattice thermal conductivities in YbAlO_3 in the quasi-one-dimensional quantum magnet regime below 1 K.

Finally we return to our motivation of gaining information on the low-temperature thermal conductivity of YAlO_3 and the effect of rare-earth ion substitution. YAlO_3 exhibits a very good thermal conductivity down to liquid helium temperatures. We found a moderate anisotropy with $\kappa_b > \kappa_c$. This allows in principle optimizing thermal properties for applications by choosing an appropriate crystal orientation. However, the influence of anisotropy is probably of minor importance compared to other aspects as realization of a good thermal coupling and crystal quality.

Replacement of Y by much heavier Yb has only a small effect on the thermal conductivity above 50 K, i.e. the regime, where umklapp scattering is dominating. An extrapolation of the measured thermal conductivity of our YbAlO_3 crystals towards lower T is not possible, as it depends sensitively on crystal size and purity. However, for Y- and Yb crystals of comparable quality the similarity above 50 K both in absolute values and T dependence of κ suggests that it extends also to lower T , as long as no magnetic contributions from Yb moments in scattering or transport become important. These effects are expected to play a role only at very low T due to the localized character of the Yb magnetic moments with an ordering temperature of below 1 K [25].

IV. SUMMARY

We have measured large thermal conductivities with weak anisotropy in single crystals of YAlO_3 and YbAlO_3 . The exchange of Y by Yb has a minor effect on κ down to 50 K despite the considerable change in density and average atomic mass. Our results on YAlO_3 confirm the suitability of the material for applications requiring a low thermal resistance, e.g., in lasers, sensors, and as substrate materials at temperatures down to liquid He.

ACKNOWLEDGMENTS

We wish to acknowledge funding from the Deutsche Forschungsgemeinschaft (DFG, German Research Foundation) through the Collaborative Research Centers SFB 1143 and TRR 80 and through the Würzburg-Dresden Cluster of Excellence EXC 2147 on Complexity and Topology in Quantum Materials - ct.qmat. We acknowledge financial support from the Max Planck Society through the Physics of Quantum Materials department and the research group "Physics of Unconventional Metals and Superconductors (PUMAS)".

DATA AVAILABILITY STATEMENT

The data that support the findings of this article are openly available [48].

-
- [1] L. Vasylechko, A. Senyshyn, and U. Bismayer, Handbook on the Physics and Chemistry of Rare Earths, edited by K. A. Gschneidner, Jr., J.-C. G. Bünzli, and V. K. Pecharsky, Vol. 39 (Elsevier, North-Holland, 2009) Chap. Perovskite-Type Aluminates and Gallates, pp. 113–295.
 - [2] J. J. Robles, A. Bartaszyte, H. P. Ng, A. Abrutis, and F. Weiss, On the possibility of growing unidirectionally twinned $\text{YBa}_2\text{Cu}_3\text{O}_{7-\delta}$ thin films on YAlO_3 , *Physica C* **400**, 36 (2003).
 - [3] Y. Uchida, K. Kaminaga, T. Fukumura, and T. Hasegawa, Samarium monoxide epitaxial thin film as a possible heavy-fermion compound, *Phys. Rev. B* **95**, 125111 (2017).
 - [4] W. Dewo, V. Gorbenko, Y. Syrotych, Y. Zorenko, and T. Runka, Mn-doped XAlO_3 ($X = \text{Y, Tb}$) single-crystalline films grown onto YAlO_3 substrates: Raman spectroscopy study toward visualization of mechanical stress, *J. Phys. Chem. C* **125**, 16279 (2021).
 - [5] C. D'Ambrosio, F. De Notaristefani, H. Leutz, D. Puertolas, and E. Rosso, Crystalline YAlO_3 as a novel window for photodetectors, *Nucl. Instr. and Meth. A* **454**, 221 (2000).
 - [6] H. Uchiyama, H. Aizawa, T. Katsumata, S. Komuro, T. Morikawa, and E. Toba, Fiber-optic thermometer using Cr-doped YAlO_3 sensor head, *Rev. Sci. Instrum.* **74**, 3883 (2003).
 - [7] M. A. Noginov, N. Noginova, M. Curley, N. Kukhtarev, H. J. Caulfield, P. Venkateswarlu, and G. B. Loutts, Optical characterization of $\text{Mn}:\text{YAlO}_3$: Material for holographic recording and data storage, *J. Opt. Soc. Am. B* **15**, 1463 (1998).

- [8] G. B. Loutts, M. Warren, L. Taylor, R. R. Rakhimov, H. R. Ries, G. Miller, M. A. Noginov, M. Curley, N. Noginova, N. Kukhtarev, H. J. Caulfield, and P. Venkateswarlu, Manganese-doped yttrium orthoaluminate: A potential material for holographic recording and data storage, *Phys. Rev. B* **57**, 3706 (1998).
- [9] F. Vittori, F. de Notaristefani, and T. Malatesta, Crystals and light collection in nuclear medicine, *Nucl. Phys. B* **78**, 616 (1999).
- [10] S. Yamamoto, N. Ukon, K. Washiyama, K. Hasegawa, K. Kamada, M. Yoshino, and A. Yoshikawa, Development of a phoswich detector composed of ZnS(Ag) and YAP(Ce) for astatine-211 imaging, *Radiat. Meas.* **153**, 106734 (2022).
- [11] E. Costa, M. N. Cinti, M. Feroci, G. Matt, and M. Rapisarda, Design of a scattering polarimeter for hard X-ray astronomy, *Nucl. Instrum. Meth. A* **366**, 161 (1995).
- [12] Y.-J. Song, N. Zong, Z.-M. Wang, Z.-Z. Chen, S.-J. Zhang, X.-J. Wang, Y. Bo, and Q.-J. Peng, High efficiency cryogenic CW Nd:YAlO₃ laser with dual wavelengths at 1072 and 1079 nm, *Opt. Laser Technol.* **163**, 109397 (2023).
- [13] S. Kishimoto and T. Yamamoto, Properties of a YAP:Ce detector for high-energy X-ray counting experiments, *Nucl. Instrum. Meth. A* **508**, 425 (2003).
- [14] R. L. Aggarwal, D. J. Ripin, J. R. Ochoa, and T. Y. Fan, Measurement of thermo-optic properties of Y₃Al₅O₁₂, Lu₃Al₅O₁₂, YAlO₃, LiYF₄, LiLuF₄, BaY₂F₈, KGd(WO₄)₂, and KY(WO₄)₂ laser crystals in the 80 – 300 K temperature range, *J. Appl. Phys.* **98**, 103514 (2005).
- [15] C. Zhang, Y. Chen, S. Ma, H. Fan, Y. Yu, Z. Hu, N. Ye, J. Wang, and Y. Wu, Thermal and fluorescence spectrum properties of Dy:YAlO₃ crystal influenced by doping concentrations, *Opt. Mater.* **138**, 113633 (2023).
- [16] R. Berman, Thermal conduction in solids (Oxford University Press, 1976).
- [17] J. Petit, B. Viana, P. Goldner, J.-P. Roger, and D. Fournier, Thermomechanical properties of Yb³⁺ doped laser crystals: Experiments and modeling, *J. Appl. Phys.* **108**, 123108 (2010).
- [18] Y. Song, N. Zong, K. Liu, Z. Wang, X. Wang, Y. Bo, Q. Peng, and Z. Xu, Temperature-dependent thermal and spectroscopic properties of Yb:YAlO₃ perovskite crystal for a cryogenically cooled near IR laser, *Opt. Mater. Express* **10**, 1522 (2020).
- [19] Y. Zhydashchikov, D. Galanciak, S. Kobayakov, M. Berkowski, A. Kamińska, A. Suchocki, Y. Zakharko, and A. Durygin, Photoluminescence studies of Mn⁴⁺ ions in YAlO₃ crystals at ambient and high pressure, *J. Phys.: Condens. Matter* **18**, 11385 (2006).

- [20] A. Senyshyn and L. Vasylechko, Low temperature crystal structure behaviour of complex yttrium aluminium oxides YAlO_3 and $\text{Y}_3\text{Al}_5\text{O}_{12}$, *Acta. Phys. Pol. A* **124**, 329 (2013).
- [21] G. A. Slack, Nonmetallic crystals with high thermal conductivity, *J. Phys. Chem. Solids* **34**, 321 (1973).
- [22] H. Xiang, Z. Feng, and Y. Zhou, Theoretical investigations on mechanical anisotropy and intrinsic thermal conductivity of YbAlO_3 , *J. Eur. Ceram. Soc.* **35**, 1549 (2015).
- [23] X. Zhan, Z. Li, B. Liu, J. Wang, Y. Zhou, and Z. Hu, Theoretical prediction of elastic stiffness and minimum lattice thermal conductivity of $\text{Y}_3\text{Al}_5\text{O}_{12}$, YAlO_3 and $\text{Y}_4\text{Al}_2\text{O}_9$, *J. Am. Ceram. Soc.* **95**, 1429 (2012).
- [24] P. Mokhtari, S. Galeski, U. Stockert, S. E. Nikitin, R. Wawrzyńczak, R. Küchler, M. Brando, L. Vasylechko, O. A. Starykh, and E. Hassinger, 1/5 and 1/3 magnetization plateaux in the spin 1/2 chain system YbAlO_3 , *Phys. Rev. Lett.* **135**, 076704 (2025).
- [25] L. S. Wu, S. E. Nikitin, Z. Wang, W. Zhu, C. D. Batista, A. M. Tsvelik, A. M. Samarakoon, D. A. Tennant, M. Brando, L. Vasylechko, M. Frontzek, A. T. Savici, G. Sala, G. Ehlers, A. D. Christianson, M. D. Lumsden, and A. Podlesnyak, Tomonaga-Luttinger liquid behavior and spinon confinement in YbAlO_3 , *Nat. Commun.* **10**, 698 (2019).
- [26] L. S. Wu, S. E. Nikitin, M. Brando, L. Vasylechko, G. Ehlers, M. Frontzek, A. T. Savici, G. Sala, A. D. Christianson, M. D. Lumsden, and A. Podlesnyak, Antiferromagnetic ordering and dipolar interactions of YbAlO_3 , *Phys. Rev. B* **99**, 195117 (2019).
- [27] O. Buryy, Y. Zhydachevskii, L. Vasylechko, D. Sugak, N. Martynyuk, S. Ubizskii, and K. D. Becker, Thermal changes of the crystal structure and the influence of thermo-chemical annealing on the optical properties of YbAlO_3 crystals, *J. Phys.: Condens. Matter* **22**, 055902 (2010).
- [28] R. Diehl and G. Brandt, Crystal structure refinement of YAlO_3 , a promising laser material, *Mater. Res. Bull.* **10**, 85 (1975).
- [29] F. Sun, S. Mishra, U. Stockert, R. Daou, N. Kikugawa, R. S. Perry, E. Hassinger, S. A. Hartnoll, A. P. Mackenzie, and V. Sunko, The Lorenz ratio as a guide to scattering contributions to transport in strongly correlated metals, *Proceedings of the National Academy of Sciences* **121**, e2318159121 (2024), <https://www.pnas.org/doi/pdf/10.1073/pnas.2318159121>.
- [30] V. Martelli, J. L. Jiménez, M. Continentino, E. Baggio-Saitovitch, and K. Behnia, Thermal transport and phonon hydrodynamics in strontium titanate, *Phys. Rev. Lett.* **120**, 125901 (2018).

- [31] D. T. Morelli, Thermal conductivity of high temperature superconductor substrate materials: Lanthanum aluminate and neodymium aluminate, *J. Mater. Res.* **7**, 2492 (1992).
- [32] W. Schnelle, R. Fischer, and E. Gmelin, Specific heat capacity and thermal conductivity of NdGaO_3 and LaAlO_3 single crystals at low temperatures, *J. Phys. D: Appl. Phys.* **34**, 846 (2001).
- [33] A. K. McCurdy, H. J. Maris, and C. Elbaum, Anisotropic heat conduction in cubic crystals in the boundary scattering regime, *Phys. Rev. B* **2**, 4077 (1970).
- [34] G. A. Slack, Thermal conductivity of MgO , Al_2O_3 , MgAl_2O_4 , and Fe_3O_4 crystals from 3 degrees to 300 degrees K, *Phys. Rev.* **126**, 427 (1962).
- [35] A. M. Hofmeister, Thermal diffusivity of oxide perovskite compounds at elevated temperature, *J. Appl. Phys.* **107**, 103532 (2010).
- [36] D. R. Clarke, Materials selection guidelines for low thermal conductivity thermal barrier coatings, *Surf. Coat. Technol.* **163-164**, 67 (2013).
- [37] V. Martelli, F. Abud, J. L. Jiménez, E. Baggio-Saitovich, L.-D. Zhao, and K. Behnia, Thermal diffusivity and its lower bound in orthorhombic SnSe , *Phys. Rev. B* **104**, 035208 (2021).
- [38] J. Suda, O. Kamishima, K. Hamaoka, I. Matsubara, T. Hattori, and T. Sato, The first-order Raman spectra and lattice dynamics for YAlO_3 crystal, *J. Phys. Soc. Jpn.* **72**, 1418 (2003).
- [39] A. Togo, Ab-initio phonon calculation for YAlO_3 / Pnma (62) / materials id 3792.
- [40] W. Voigt, Lehrbuch der Kristallphysik (Teubner, Leipzig, 1928).
- [41] A. Reuss, Berechnung der Fließgrenze von Mischkristallen auf Grund der Plastizitätsbedingung für Einkristalle, *Z. Angew. Math. Mech.* **9**, 49 (1929).
- [42] R. Hill, The elastic behaviour of a crystalline aggregate, *Proc. Phys. Soc. A* **65**, 349 (1952).
- [43] G. A. Slack and S. Galginaitis, Thermal conductivity and phonon scattering by magnetic impurities in CdTe , *Phys. Rev.* **133**, A253 (1964).
- [44] J. Callaway, Model for lattice thermal conductivity at low temperatures, *Phys. Rev.* **113**, 1046 (1959).
- [45] M. G. Holland, Analysis of lattice thermal conductivity, *Phys. Rev.* **132**, 2461 (1963).
- [46] M. Asen-Palmer, K. Bartkowski, E. Gmelin, M. Cardona, A. P. Zhernov, A. V. Inyushkin, A. Taldenkov, V. I. Ozhogin, K. M. Itoh, and E. E. Haller, Thermal conductivity of germanium crystals with different isotopic compositions, *Phys. Rev. B* **56**, 9431 (1997).
- [47] P. B. Allen, Improved Callaway model for lattice thermal conductivity, *Phys. Rev. B* **88**, 144302 (2013).

- [48] P. Mokhtari, U. Stockert, S. Nikitin, L. Vasylechko, M. Brando, and E. Hassinger, Data sets "Low-temperature thermal conductivity of the substrate material YAlO_3 and its unconventional sister compound YbAlO_3 ", Technische Universität Dresden, 2025, <https://doi.org/10.25532/OPARA-949>.